This article has been accepted for inclusion in a future issue of this journal. Content is final as presented, with the exception of pagination.

High-Speed and Responsivity 4H-SiC 8×8 p-i-n Ultraviolet Photodiode Arrays With Micro-Hole Structure

Zhao Fu, Mingkun Zhang, Shan Han, Jiafa Cai, Rongdun Hong, Xiaping Chen, Dingqu Lin, Shaoxiong Wu, Yuning Zhang, Deyi Fu, Zhengyun Wu, Baoping Zhang, Feng Zhang, *Member, IEEE*, and Rong Zhang

***Abstract*—In this brief, high-performance 8×8 arrays of 4H-SiC p-i-n ultraviolet (UV) photodiodes (PDs) with micro-hole structure are demonstrated. In order to improve the performance of the device, a periodic micro-hole structure (diameter = 4 μm) was etched from the cap layer (p^+ layer) to the i layer, which will elevate the effective absorption of UV light. The pixels in 4H-SiC p-i-n array show a low dark current of less than 2×10^{-14} A and a high yield of 98.4%. Devices with 4-μm micro-hole reach a peak spectral responsivity of 0.159 A/W at 280 nm, which is 23.3% higher than that of the device without micro-hole. Moreover, the device has a faster response time of 2.2 ns and a high UV/visible rejection ratio of more than 10^4. The progress on the response performance is significant to the development of UV detection imaging.**

Manuscript received 24 April 2023; revised 4 June 2023; accepted 9 June 2023. This work was supported in part by the National Natural Science Foundation of China under Grant 62274137; in part by the Natural Science Foundation of Fujian of China for Distinguished Young Scholars under Grant 2020J06002; in part by the Natural Science Foundation of Jiangxi of China for Distinguished Young Scholars under Grant S2021QNZD2L0013; in part by the Science and Technology Project of Fujian of China under Grant 2020I0001; in part by the Science and Technology Key Projects of Xiamen under Grant 3502ZCQ20191001; in part by the Laboratory Open Fund of Beijing Smart-Chip Microelectronics Technology Company Ltd., under Grant SGSC0000KJQT2207192; in part by the Fundamental Research Funds for the Central Universities under Grant 20720220026; in part by the Shenzhen Science and Technology Program under Grant JSGG20201102155800003; and in part by the Jiangxi Provincial Natural Science Foundation under Grant 20212ACB212005. The review of this brief was arranged by Editor S. Long. *(Corresponding authors: Mingkun Zhang; Feng Zhang; Rong Zhang.)*

Zhao Fu, Shan Han, Jiafa Cai, Rongdun Hong, Xiaping Chen, Dingqu Lin, Shaoxiong Wu, Yuning Zhang, Deyi Fu, Zhengyun Wu, and Feng Zhang are with the Department of Physics, College of Physical Science and Technology, Xiamen University, Xiamen 361005, China (e-mail: fzhang@xmu.edu.cn).

Mingkun Zhang is with the Department of Physics, College of Physical Science and Technology, and the School of Electronic Science and Engineering, Xiamen University, Xiamen 361005, China (e-mail: mkzhang@xmu.edu.cn).

Baoping Zhang is with the School of Electronic Science and Engineering, Xiamen University, Xiamen 361005, China.

Rong Zhang is with the Department of Physics, College of Physical Science and Technology, Xiamen University, Xiamen 361005, China, and also with the School of Electronic Science and Engineering, Nanjing University, Nanjing 210093, China (e-mail: rzhangxmu@xmu.edu.cn).

Color versions of one or more figures in this article are available at https://doi.org/10.1109/TED.2023.3286379.

Digital Object Identifier 10.1109/TED.2023.3286379

***Index Terms*—4H-SiC, array, micro-hole, p-i-n, photodiode (PDs), ultraviolet (UV).**

I. Introduction

ULTRAVIOLET (UV) photodiodes (PDs) based on wide bandgap materials (such as 4H-SiC, GaN, and diamond) have numerous applications in various areas, such as chemical sensing, solar UV monitoring, secure space-to-space communication, and flame detection [1], [2], [3], [4]. 4H-SiC is regarded as the most suitable for UV detection, due to the good material quality and wide bandgap 3.26 eV (384-nm cutoff) [5], which is naturally transparent to visible and infrared light. The 4H-SiC-based UV PDs with various structures have been reported, including Schottky [6], metal-semiconductor-metal (MSM) [7], p-i-n [8], [9], and avalanche structure [10]. Due to the high photogenerated carrier collection efficiency, low dark current, and high response speed, 4H-SiC p-i-n PDs have gradually become a hot topic in the field of optoelectronics in recent years. Recently, the development of 4H-SiC p-i-n PDs mainly focuses on two aspects: one is to improve the fabrication technology or structure to enhance the performance [11], [12], [13], [14] and the other is the development of large area array [15], [16], [17], [18]. The p-i-n 2-D arrays are desirable for such applications as spectroscopy and UV imaging, which will be one of the development trends for 4H-SiC UV PDs.

In this brief, in order to achieve high efficiency and speed UV imaging, the response of single pixel is improved by using a micro-hole structure, and a larger area of 8×8 4H-SiC p-i-n PD with high yield and uniformity is demonstrated in this work.

II. Device Structure and Fabrication

Fig. 1(a) shows the top-view microscope image of the whole 4H-SiC 8×8 p-i-n with micro-hole, and the single pixel of the 8×8 p-i-n array is shown in Fig. 1(b). The photoactive window area of single pixel is 200×200 μm^2 and the distance between each pixel is 200 μm. The total size of the p-i-n array is 3.7×3.7 mm^2. The cross section of the micro-hole p-i-n device with thickness and doping profiles is shown

0018-9383 © 2023 IEEE. Personal use is permitted, but republication/redistribution requires IEEE permission.
See https://www.ieee.org/publications/rights/index.html for more information.

Authorized licensed use limited to: Xiamen University. Downloaded on July 06,2023 at 02:36:00 UTC from IEEE Xplore. Restrictions apply.

This article has been accepted for inclusion in a future issue of this journal. Content is final as presented, with the exception of pagination.

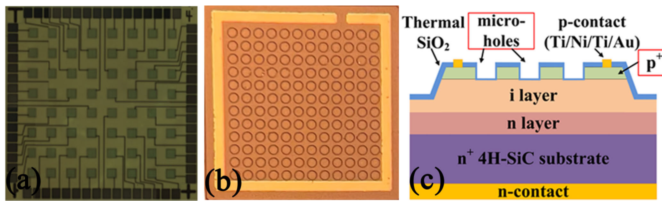

Fig. 1. (a) Microscope image of the whole 4H-SiC 8 × 8 p-i-n with micro-hole. (b) SEM image of single pixel of the 8 × 8 p-i-n array. (c) Schematic of 4H-SiC p-i-n device structure shows the doping concentration of each layer.

in Fig. 1(c). The homoepitaxy layers were grown in sequence on a low-defect-density n$^+$-doped 4H-SiC substrate, including a 500-nm n-layer ($N_D = 2 \times 10^{18}$ cm^{-3}), a 1000-nm i layer ($N = 1 \times 10^{15}$ cm^{-3}), and a 200-nm p$^+$ layer ($N_A = 1 \times 10^{19}$ cm^{-3}).

First, the beveled mesa was etched by inductive coupled plasma (ICP) based on photoresist reflow technology. Then, the micro-holes with the diameter of 4 μm and the spacing of 5 μm were prepared by a standard photolithography and ICP etching. The ICP etching was performed at 10° with a 30-sccm (CF_4)/5-sccm (O_2) gas flow rate, and the etching rate was controlled at 0.8 ± 0.1 nm/s. By controlling the etching time, micro-hole with the depth of 220 ± 10 nm is obtained by atomic force microscope (AFM). It ensures that the micro-holes are etched to the i layer, which allows more UV light to be absorbed directly by the i layer. Then, a thermally grown SiO_2 (~45 nm) was deposited on the surface to reduce the leakage current of the device and suppress the edge breakdown of micro-holes. Ohmic contact metals on the p$^+$ layer and the backside of n$^+$ substrate are obtained by Ti/Al/Ti/Au (40/60/10/100 nm) and Ti/Ni/Ti/Au (5/200/5/150 nm), respectively, followed by a rapid thermal annealing process of 1000 °C/2 min in Ar ambient. Finally, Ti/Au (20/300 nm) was sputtered as a wire-bonding pad. The traditional 4H-SiC p-i-n PD array without micro-hole was also fabricated for comparison.

The current–voltage (I–V) characteristics were performed by the Keithley 4200-SCS parameter analyzer. A Xenon lamp as an output light source was used in the spectral response measurement. The output light was dispersed through a monochromator for wavelength selection and focused onto the sample by lens. The incident light power was calibrated by a Si-based detector in the wavelength range of 200–400 nm. In order to measure the response speed, the PD was biased using Keithley 2410, and the voltage transient response of the PD was measured using an oscilloscope (Tektronix MSO44). The light with a wavelength of 266 nm is excited by using a picosecond laser pulse, with a pulsewidth of 10 ps and a recurrence frequency of 1×10^6 Hz.

III. Results and Discussion

Fig. 2(a) shows the reverse I–V characteristics of the devices with and without micro-hole (4 and 8 μm) under dark. It is clear that the dark current is relatively stable in the reverse bias range of 0–20 V and less than 1×10^{-14} A, corresponding to a current density of ~25 pA/cm^2. Despite the

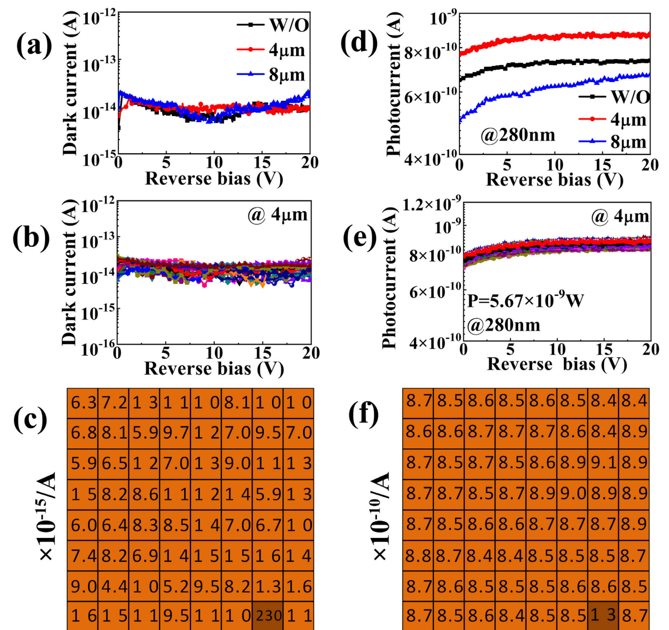

Fig. 2. (a) Reverse I–V characteristics of the devices without and with 4- and 8-μm micro-hole under dark. Uniformity of 4H-SiC 8 × 8 p-i-n PD array with 4-μm micro-hole: (b) dark I–V characteristics of pixels and (c) 2-D mapping of dark current of each pixel in an 8 × 8 array. (d) Reverse I–V characteristics of the devices without and with 4- and 8-μm micro-hole arrays under the illumination of 280 nm. (e) Photocurrent–voltage characteristics of pixels in an 8 × 8 array. (f) Two-dimensional mapping of photocurrent of each pixel in an 8 × 8 array.

etching of micro-hole structure, the passivation layer deposited on the surface suppresses the leakage at the edge of the micro-hole effectively and contributes a low dark current. It is well known that the uniformity of each pixel in the same detector array is of great significance for imaging and other applications. Therefore, the uniformity of 4H-SiC 8 × 8 p-i-n array with 4-μm micro-hole is analyzed. Fig. 2(b) shows the dark I–V characteristics of different pixels in a 4H-SiC 8 × 8 p-i-n array with 4-μm micro-hole, and the corresponding 2-D mapping of dark current of each pixel in an 8 × 8 array is shown in Fig. 2(c). It is easy to find that the pixels show a high uniformity and a low dark current of less than 2×10^{-14} A, except the pixel 2.3×10^{-13} of the eighth row and seventh column. If the one pixel with large dark current is regarded as a "bad" one, the corresponding pixel yield is 98.4%. Considering elementary screw dislocations in present 4H-SiC epitaxial layer, the high yield of 98.4% of 8 × 8 array is very meaningful.

Fig. 2(d) shows the reverse I–V characteristic curves of devices without and with 4- and 8-μm micro-hole under illumination at 280 nm with an optical power of 5.67×10^{-9} W. On the one hand, the device with 4-μm micro-hole achieves the largest photocurrent compared to the device with and without 8-μm micro-hole under the same illumination since more light is absorbed directly by the i layer and depleted at micro-hole completely. On the other hand, the reason for the minimum photocurrent of the device with 8-μm micro-hole can be attributed to the fact that the electric field at micro-hole cannot be completely depleted. It is indicated that

Authorized licensed use limited to: Xiamen University. Downloaded on July 06,2023 at 02:36:00 UTC from IEEE Xplore. Restrictions apply.

This article has been accepted for inclusion in a future issue of this journal. Content is final as presented, with the exception of pagination.

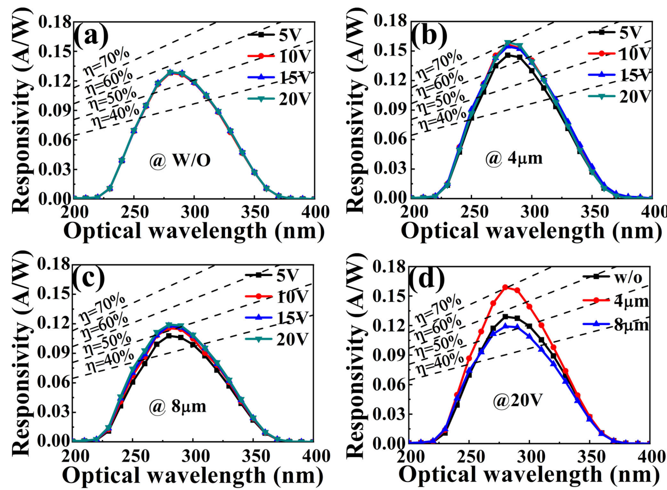

Fig. 3. Spectral response curves of the devices in the voltage range of 5–20 V. (a) Without micro-hole. (b) With 4-μm micro-hole. (c) With 8-μm micro-hole. (d) Spectral response and external quantum efficiency curve of devices with and without micro-hole at 20-V bias.

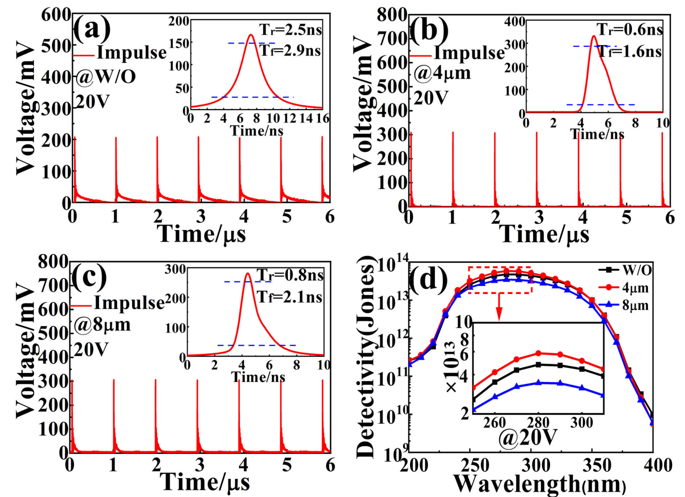

Fig. 4. Response speed of the device at 20 V, the inset is a magnified of a single impulse. (a) Without micro-hole. (b) With 4-μm micro-hole. (c) With 8-μm micro-hole. (d) Corresponding detectivity with the wavelength range from 200 to 400 nm and the inset shows detectivity from 250 to 310 nm.

the photocurrent also shows the same uniformity as the dark current from Fig. 2(e) and (f). All of pixels show a uniform response for UV light except the pixel of the eighth row and seventh column, which is of great significance to UV imaging.

Furthermore, the spectral response of devices with and without micro-hole (4 and 8 μm) under different reverse biases is analyzed. Fig. 3(a) shows that the peak responsivity of the device without micro-hole hardly changes with the reverse bias gradually increased from 5 to 20 V, which is normal for 4H-SiC PDs because the absorber layer is completely depleted under a low bias voltage of 5 V. Fig. 3(b) shows that the peak responsivity of the device with 4-μm micro-hole increased significantly from 0.146 to 0.159 A/W with the reverse bias increased from 5 to 10 V and changes less with the reverse bias increased from 10 to 20 V. Since there is no p^+ layer in the micro-hole, the depletion area of the absorption layer at the micro-hole mainly depends on the lateral depletion of the p^+ layer at the micropore spacing. As for the device with 4-μm micro-hole, it means that the absorption layer at the micro-hole is not completely depleted in the horizontal direction at 5-V reverse bias and is completely depleted when the reverse bias exceeds 10 V. Fig. 3(c) shows that the change trend of the device with 8-μm micro-hole is similar to Fig. 3(b), but the difference is that the increasing trend of peak responsivity just slows down and the peak responsivity 0.119 A/W is far less than the peak responsivity 0.159 A/W of the device with 4-μm micro-hole when the reverse bias is greater than 10 V, which is attribute to that the diameter of micro-hole is too wide to be depleted in the horizontal direction even when the bias voltage is increased to 20 V, and the free electron–hole pairs cannot be quickly collected by the electrode and is easy to be recombined by defects. The above theories and simulation about the depletion region at MH can refer to our previous work in detail [19]. It can be obtained from Fig. 3(d) that the peak responsivity and corresponding external quantum efficiency of the device with 4-μm micro-hole achieve 0.159 A/W and 70.1% at 20 V reversed bias, respectively, which are increased by 23.3% compared to those of the device without micro-hole.

Fig. 4(a)–(c) shows the response speed of the device without micro-hole, and with 4- and 8-μm micro-hole, respectively. The response time is defined as the sum of the rise time (T_r) and fall time (T_f) (T_r and T_f are defined as the time during which the impulse voltage rises from 10% to 90% and falls from 90% to 10% of the peak value, respectively). From the inset, it can be seen that the response time of device with micro-hole arrays is slightly faster than that of the device without micro-hole and the response time is 2.2 ns for the device with 4-μm micro-hole. It is indicated that the response time has been reduced 59.3%, which may be due to the fact that light is directly absorbed by the depletion layer, reducing the drift time. It also finds that the device with 4-μm micro-hole has a slightly shorter rise time and fall time than that with 8-μm micro-hole, which may be attributed the fact that the carriers cannot drift in the incomplete depletion region of the micro-hole but eventually be collected through diffusion.

The responsivity (R) and detectivity ($D*$) can be calculated by the following formulas [20], [21]:

$$R = \frac{I_p}{P_{\text{opt}}} = \frac{I_{\text{ph}} - I_d}{P_{\text{opt}}} \quad (1)$$

$$D^* = R \cdot \sqrt{S/(2eI_d)} \quad (2)$$

where I_{ph} and I_d represent the photocurrent and dark current of PDs, respectively and P_{opt} is the optical power in watts. I_{ph} is four orders of magnitude larger than I_d for any PDs ($I_{\text{ph}} - I_d \approx I_{\text{ph}}$), and therefore, R depends linearly on I_{ph}. S is the photosensitive area of the device.

Fig. 4(d) shows the comparison of the detectivity for the devices with and without micro-hole at 20-V reverse bias. The device with 4-μm micro-hole achieved the highest detectivity of 5.9 × 10^{13} Jones at 280 nm, which is higher than other devices due to its higher responsivity and lower dark current.

Authorized licensed use limited to: Xiamen University. Downloaded on July 06,2023 at 02:36:00 UTC from IEEE Xplore. Restrictions apply.

This article has been accepted for inclusion in a future issue of this journal. Content is final as presented, with the exception of pagination.

TABLE I
SUMMARY OF PERFORMANCE PARAMETERS OF 4H-SiC p-i-n PDs

Dark current density (nA/cm^2)	R (A/W)	D*(Jones)	References
0.025	0.159	5.9×10^{13}	this work
1.0	0.11	6.2×10^{12}	[11]
1.0	0.14	7.84×10^{12}	[12]
38.6	0.188	1.69×10^{12}	[13]
3.9×10^3	0.078	7.0×10^{10}	[14]
0.025	0.14	4.2×10^{13}	[18]

Table I shows the performance parameters of the prepared 4H-SiC p-i-n PDs and compares them with those prepared by other groups. Considering dark current density and responsivity, this work has the highest detectivity, which is a very important performance parameter for PDs.

IV. CONCLUSION

In this brief, 4H-SiC 8 × 8 p-i-n UV PD arrays with periodic micro-hole structure were reported, which obtained a high yield of 98.4% and a high uniformity of low dark current. As for single pixel, the device with 4-μm micro-hole obtained the highest peak responsivity of 0.159 A/W at 20-V reverse bias, corresponding external quantum efficiency of 70.1%, which is 23.3% higher than the device without micro-hole. Meanwhile, the fast response time of 2.2 ns is the improvement of 59.3%. The new structure of micro-hole is beneficial to improve the performance of the device. High yield and uniformity of 4H-SiC 8 × 8 p-i-n PD array are significant to UV detection imaging.

REFERENCES

[1] M. Kim, J.-H. Seo, U. Singisetti, and Z. Ma, "Recent advances in free-standing single crystalline wide band-gap semiconductors and their applications: GaN, SiC, ZnO, βGa_2O_3, and diamond," *J. Mater. Chem. C*, vol. 5, no. 33, pp. 8338–8354, Sep. 2017.

[2] H. Chen, K. Liu, L. Hu, A. A. Al-Ghamdi, and X. Fang, "New concept ultraviolet photodetectors," *Mater. Today*, vol. 18, no. 9, pp. 493–502, Nov. 2015, doi: 10.1016/j.mattod.2015.06.001.

[3] Z. Alaie, S. M. Nejad, and M. H. Yousefi, "Recent advances in ultraviolet photodetectors," *Mater. Sci. Semicond. Process.*, vol. 29, pp. 16–55, Jan. 2015, doi: 10.1016/j.mssp.2014.02.054.

[4] M. Razeghi, "Short-wavelength solar-blind detectors-status, prospects, and markets," *Proc. IEEE*, vol. 90, no. 6, pp. 1006–1014, Jun. 2002, doi: 10.1109/JPROC.2002.1021565.

[5] E. Monroy, F. Omn S, and F. Calle, "Wide-bandgap semiconductor ultraviolet photodetectors," *Semicond. Sci. Technol.*, vol. 18, no. 4, pp. R33–R51, Apr. 2003, doi: 10.1088/0268-1242/18/4/201.

[6] Z. Wang et al., "High-performance 4H-SiC Schottky photodiode with semitransparent grid-electrode for EUV detection," *IEEE Photon. Technol. Lett.*, vol. 32, no. 13, pp. 791–794, Jul. 1, 2020, doi: 10.1109/LPT.2020.2996308.

[7] Y. K. Su, Y. Z. Chiou, C. S. Chang, S. J. Chang, Y. C. Lin, and J. F. Chen, "4H-SiC metal-semiconductor-metal ultraviolet photodetectors with Ni/ITO electrodes," *Solid-State Electron.*, vol. 46, no. 12, pp. 2237–2240, Dec. 2002, doi: 10.1016/S0038-1101(02)00234-4.

[8] X. Chen, H. Zhu, J. Cai, and Z. Wu, "High-performance 4H-SiC-based ultraviolet p-i-n photodetector," *J. Appl. Phys.*, vol. 102, no. 2, Jul. 2007, Art. no. 024505, doi: 10.1063/1.2747213.

[9] Y. Hou et al., "Effect of epitaxial layer's thickness on spectral response of 4H-SiC p-i-n ultraviolet photodiodes," *Electron. Lett.*, vol. 55, no. 4, pp. 216–217, Feb. 2019, doi: 10.1049/el.2018.8035.

[10] M. K. Zhang, K. L. Wang, H. X. Jiang, R. D. Hong, and Z. Y. Wu, "High performance silicon carbide avalanche-p-i-n ultraviolet photodiode with dual operation models," *Electron. Lett.*, vol. 52, no. 17, pp. 1474–1475, Aug. 2016, doi: 10.1049/el.2016.2025.

[11] A. Sciuto, M. Mazzillo, S. Di Franco, F. Roccaforte, and G. D'Arrigo, "Visible blind 4H-SiC p^+-n UV photodiode obtained by Al implantation," *IEEE Photon. J.*, vol. 7, no. 3, pp. 1–6, Jun. 2015, doi: 10.1109/JPHOT.2015.2439955.

[12] S. Yang et al., "High-performance 4H-SiC p-i-n ultraviolet photodiode with P layer formed by Al implantation," *IEEE Photon. Technol. Lett.*, vol. 28, no. 11, pp. 1189–1192, Jun. 1, 2016, doi: 10.1109/LPT.2016.2535407.

[13] M. L. Megherbi et al., "An efficient 4H-SiC photodiode for UV sensing applications," *Electronics*, vol. 10, no. 20, p. 2517, Oct. 2021, doi: 10.3390/electronics10202517.

[14] S. Guo et al., "Visible-blind photodetector based on p-i-n junction 4H-SiC vertical nanocone array," *IEEE Trans. Electron Devices*, vol. 68, no. 12, pp. 6208–6215, Dec. 2021, doi: 10.1109/TED.2021.3117193.

[15] X. Chen, W. Yang, and Z. Wu, "Visible blind p-i-n ultraviolet photodetector fabricated on 4H-SiC," *Microelectron. Eng.*, vol. 83, no. 1, pp. 104–106, Jan. 2006, doi: 10.1016/j.mee.2005.10.034.

[16] X. Zhou et al., "High-uniformity 1 × 64 linear arrays of silicon carbide avalanche photodiode," *Electron. Lett.*, vol. 56, no. 17, pp. 895–897, Aug. 2020, doi: 10.1049/el.2020.1241.

[17] C. D. Matthus, A. J. Bauer, L. Frey, and T. Erlbacher, "Wavelength-selective 4H-SiC UV-sensor array," *Mater. Sci. Semicond. Process.*, vol. 90, pp. 205–211, Feb. 2019, doi: 10.1016/j.mssp.2018.10.019.

[18] S. Hou, P.-E. Hellstrom, C.-M. Zetterling, and M. Ostling, "550 °C 4H-SiC p-i-n photodiode array with two-layer metallization," *IEEE Electron Device Lett.*, vol. 37, no. 12, pp. 1594–1596, Dec. 2016, doi: 10.1109/LED.2016.2618122.

[19] Z. Fu et al., "Local avalanche effect of 4H-SiC p-i-n ultraviolet photodiodes with periodic micro-hole arrays," *IEEE Electron Device Lett.*, vol. 43, no. 1, pp. 64–67, Jan. 2022, doi: 10.1109/LED.2021.3132415.

[20] M. Razeghi and A. Rogalski, "Semiconductor ultraviolet detectors," *J. Appl. Phys.*, vol. 79, pp. 7433–7473, Jan. 1996, doi: 10.1063/1.362677.

[21] R. F. Tang et al., "Localized surface plasmon enhanced Ga_2O_3 solar blind photodetectors," *Opt. Exp.*, vol. 28, no. 4, pp. 5731–5740, Feb. 2020, doi: 10.1364/oe.380017.

Authorized licensed use limited to: Xiamen University. Downloaded on July 06,2023 at 02:36:00 UTC from IEEE Xplore. Restrictions apply.